DEVELOPMENT OF SILICON AND SILICON CARBIDE NANOSTRUCTURES FOR PHOTONIC APPLICATIONS

By:

NIMA NADERI

Thesis submitted in fulfillment of the requirements for the degree of Doctor of Philosophy

UNIVERSITI SAINS MALAYSIA

July 2013

ACKNOWLEDGMENTS

I am deeply thankful to my supervisor, Professor Dr. Md Roslan Hashim, for his creative guidance, intellectual support, stimulating discussions, and inspiring words. I am also grateful for his excellent hospitality and wonderful attitude.

I acknowledge the Universiti Sains Malaysia (USM) Fellowship program for its financial support to this research. I express my gratitude as well to all staff members of the School of Physics, USM for their encouragement.

I also express appreciation to the staff of the Nano-Optoelectronics Research and Technology Laboratory (NOR Lab) and of the Solid-state Laboratory for their technical assistance during my laboratory work, particularly in the sample characterizations.

My heartfelt gratitude also goes to my family members: to my father and mother for their continuous prayers and support, and to my brothers for their encouragement. Words cannot sufficiently express how grateful I feel. Finally, I thank all who supported me in any respect during the completion of this study.

Nima Naderi

July 2013

Penang – Malaysia

TABLE OF CONTENTS

ACKNOWLEDGMENTS ii

TABLE OF CONTENTS iii

LIST OF TABLES viii

LIST OF FIGURES ix

LIST OF SYMBOLS xiv

LIST OF MAJOR ABBREVIATIONS xvi

ABSTRAK xviii

ABSTRACT xix

CHAPTER 1: INTRODUCTION 1

1.1 Fundamentals of Compound Semiconductors and Silicon Carbide 1

1.2 Overview and Background of Porous Silicon and Porous SiC Nanostructures . 4

1.3 Overview and Background of SiC Growth Techniques 7

1.3.1 Liquid Phase Epitaxy (LPE) 8

1.3.2 Chemical Vapor Deposition (CVD) 9

1.3.3 Molecular Beam Epitaxy (MBE) 10

1.3.4 Physical Vapor Deposition (PVD) 11

1.4 Overview of Semiconductor Photodetectors 12

1.5 Problem Statement 14

1.6 Research Objectives 15

1.7 Scope of Study 16

1.8 Outline of Thesis 16

CHAPTER 2: LITERATURE REVIEW 17

2.1 Introduction 17

2.2 Principles of Photoelectrochemical Etching 17

2.2.1 Photoelectrochemical Etching Mechanism of Silicon 18

2.2.2 Combinational Pulsed-Current Etching of Silicon 22

2.2.3 Principles of Photoelectrochemical Etching of SiC 24

2.2.4 Pulsed-Current UV-Assisted Photoelectrochemical Etching of SiC 25

2.3 Sputter Deposition 26

2.3.1 Theory of Sputter Deposition 26

2.3.2 Sputtering System 28

2.3.3 Sputtering Parameters 30

2.4 Theory of Thermal Annealing Process 32

2.5 Theory of X-Ray Crystallography 33

2.5.1 Bragg's Law 33

2.5.2 Lattice Parameters 34

2.5.3 Lattice Strain 35

2.5.4 Crystallite Size 36

2.6 Theory of Metal-Semiconductor Contacts 37

2.6.1 Ideal Metal-Semiconductor Contacts 38

2.6.2 Schottky Barrier Height 39

2.6.3 Thermionic Emission Theory 40

2.7 Metal-Semiconductor-Metal Photodetectors 41

2.7.1 Current Gain 42

2.7.2 Responsivity 42

2.7.3 Quantum efficiency 43

2.7.4 Response Time and Recovery Time 43

CHAPTER 3: METHODOLOGY 45

3.1 Introduction 45

3.2 Preparation of Substrates ... 46

3.3 Method for Deposition of Metal Back Contacts ... 47

3.3.1 Thermal Evaporation ... 47

3.3.2 Thermal Annealing Furnace ... 48

3.4 Electrochemical Analysis of Etching Process ... 49

3.5 Formation of Porous Substrates ... 51

3.5.1 Method of Generating Porous Silicon ... 52

3.5.2 Method of Generating Porous Silicon Carbide ... 54

3.6 Method of Thermal Carbonization of Porous Silicon ... 55

3.7 RF Sputtering of SiC on TC-PS Substrates ... 55

3.8 Thermal Annealing of SiC/TC-PS samples ... 56

3.9 Methods of Metallization ... 57

3.10 Characterization of MSM Photodetectors ... 58

3.11 Principles of the Characterization Tools ... 58

3.11.1 The Structural Properties Tools ... 59

3.11.2 The Optical Characterization Methods ... 63

3.11.3 The Electrical Characterizations ... 68

3.12 Summary ... 69

CHAPTER 4: STABLE POROUS SILICON ... 70

4.1 Introduction ... 70

4.2 Electrochemical Analysis for the Anodic Etching of Silicon ... 70

4.3 The Combinational Etching of Silicon (The Effect of Delay Time) ... 72

4.3.1 Surface Porosity ... 72

4.3.2 Surface Morphology ... 72

4.3.3 Photoluminescence (PL) Spectra ... 73

4.3.4 Raman Analysis 75

4.3.5 Fourier Transform Infrared (FT-IR) Analysis 77

4.3.6 Porous Silicon MSM Photodetector 78

4.3.7 Response and Recovery Time of PS Photodetectors 81

4.4 The Study of Thermal Carbonization of Porous Silicon 82

4.4.1 Thickness Measurement of Carbonized PS layer 83

4.4.2 Surface Morphology 84

4.4.3 Energy Dispersive X-ray (EDX) Spectroscopy 84

4.4.4 Fourier Transform Infrared (FT-IR) Analysis 85

4.4.5 Photoluminescence (PL) Spectra 86

4.4.6 Electrical Stability of TC-PS Photodetectors 88

4.5 Summary 91

CHAPTER 5: POROUS SILICON CARBIDE 93

5.1 Introduction 93

5.2 Electrochemical Analysis for the Anodic Etching of SiC 93

5.3 Pulsed-Current Etching of SiC (The Effect of Current Density) 95

5.3.1 Surface Porosity 95

5.3.2 Surface Morphology 96

5.3.3 Atomic Force Microscopy 97

5.3.4 UV-Visible Spectroscopy 98

5.3.5 Photoluminescence (PL) Spectra 100

5.3.6 Raman Analysis 102

5.3.7 Porous Silicon Carbide MSM UV Photodetector 104

5.4 Summary 109

CHAPTER 6: SPUTTERED POROUS-SHAPED SILICON CARBIDE 111

6.1 Introduction........ 111

6.2 The Effect of TC-PS Template 111

6.3 The Effect of Annealing Temperature 113

6.3.1 Surface Morphology 113

6.3.2 Energy Dispersive X-ray (EDX) Spectroscopy........ 116

6.3.3 Atomic Force Microscopy 117

6.3.4 X-ray Diffractometry 117

6.3.5 Optical Reflectometry........ 119

6.3.6 Photoluminescence (PL) Spectra 121

6.3.7 Raman Analysis 123

6.3.8 Porous-Shaped SiC/TC-PS MSM UV Photodetector........ 125

6.4 Summary........ 130

CHAPTER 7: CONCLUSIONS AND FUTURE DIRECTION 132

7.1 Conclusions 132

7.2 The Novelties and Benefits of this Research........ 136

7.3 Future Direction........ 136

REFERENCES........ 137

APPENDICES 150

Appendix 1: Measurements of Porosity by Weighing Method........ 150

Appendix 2: Quantum Confinement Theory........ 151

Appendix 3: XRD Standard Database (ICDD, PDF-4, 00-005-0565)........ 153

Appendix 4: XRD Standard Database (ICDD, PDF-4, 00-002-1464)........ 154

LIST OF PUBLICATIONS........ 155

LIST OF TABLES

Table 1.1. Physical properties of major SiC polytypes [12]. 3

Table 4.1. A detail of PL peaks for PS samples generated by different delay times 75

Table 4.2. The phonon modes detected in the Raman spectra 77

Table 4.3. The electrical characteristics of fabricated PS photodetectors.................. 80

Table 4.4. The photoelectrical performance of Ni/PS/Si photodetectors with different values of delay time (T_d) for a constant voltage of 5 V 82

Table 5.1. Details of the PL peaks of 6H-SiC and the PSC samples fabricated with different etching current densities 101

Table 5.2. Peak positions, peak shift, full-width at half-maximum (FWHM), and intensity of the Raman emissions of the 6H-SiC and PSC samples 103

Table 5.3. Schottky barrier height (φ_B) and ideality factor (n) of Ni/PSC/SiC UV photodetectors with different etching current densities.................. 106

Table 5.4. The electrical properties of PSC UV photodetectors with different etching current densities.. 109

Table 6.1. Crystallite size (D), lattice spacing (d-spacing), lattice constants (a and c), and calculated strain values determined for the SiC samples with different annealing temperatures.. 119

Table 6.2. Details of the PL peaks for TC-PS and SiC/TC-PS samples before and after annealing with different temperatures.................................... 123

Table 6.3. The details of A_1 (LO) mode of Raman spectra for sputtered SiC thin films on TC-PS substrate.. 125

Table 6.4. Schottky barrier height (φ_B) and ideality factor (n) of Ni/SiC/TC-PS photodetectors with different annealing temperatures 127

Table 6.5. The electrical properties of Ni/SiC/TC-PS photodetectors with different annealing temperatures 130

LIST OF FIGURES

Figure 1.1. Structure of SiC polytypes 2

Figure 2.1. Typical *J–V* spectra of silicon in dilute aqueous HF solution. The porous layer is obtainable for $J < J_{ep}$. Adopted and redrawn from [64] 19

Figure 2.2. Schematic of the chemical dissolution mechanism of Si in HF solution. Adopted and redrawn from [65] 21

Figure 2.3. RF sputtering setup for physical vapor deposition of SiC films 29

Figure 2.4. Schematic of constructive (left figure) or destructive (right figure) interferences according to the 2θ deviation in Bragg's law 34

Figure 2.5. Formation of Schottky barrier between metal and n-type semiconductor: (a) neutral and electrically isolated, (b) in ideal contact 38

Figure 2.6. Basic structure of an MSM photodetector: (a) top and (b) cross-sectional views 41

Figure 2.7. Cyclic performance of a typical photodetector which was exposed to a typical pulsed source of photon 44

Figure 3.1. Methodology and fabrication processes 45

Figure 3.2. The RCA procedures for chemical cleaning 46

Figure 3.3. Schematic of a resistive thermal evaporation system (a); Image of the Edward Auto 306 thermal evaporation vacuum coater unit (b) 48

Figure 3.4. Schematic of a thermal annealing tube furnace (a); Annealing tube furnace model Lenton VTF/12/60/700 (b) 49

Figure 3.5. Typical excitation signal for cyclic voltammetry 50

Figure 3.6. Potentiostat system, electrochemical cells, and electrodes 50

Figure 3.7. Schematic of the electrochemical analysis setup for the electrochemical characterization of the anodic etching 51

Figure 3.8. Waveform for the pulse current used in the photoelectrochemical etching of silicon and silicon carbide substrates 52

Figure 3.9. Schematic of the electrochemical etching cell used to generate porous silicon 53

Figure 3.10. Experimental setup for pulsed photoelectrochemical etching of Si 53

Figure 3.11. Schematic of the UV-assisted electrochemical etching cell used to generate porous SiC 54

Figure 3.12. Experimental setup for pulsed UV-assisted electrochemical etching of 6H-SiC.. 55

Figure 3.13. Image of the RF sputtering equipment (a); sample holder containing TC-PS substrates and SiC target (b)..................................... 56

Figure 3.14. Schematic of the co-planar metal contact used in Schottky MSM photodetectors (a); finger-shaped metal mask containing an SiC substrate (b)... 57

Figure 3.15. Image of the high-resolution XRD equipment model PANalytical X'pert PRO MRD PW3040 (a); A typical XRD pattern including peak position and peak width (b). 60

Figure 3.16. A schematic of SEM configuration (a); Scanning electron microscope and energy dispersive X-ray spectroscope (b)..................... 61

Figure 3.17. A schematic of atomic force microscopy (AFM) configuration (a); AFM system model Dimension edge, Bruker (b) 62

Figure 3.18. A schematic of Raman spectroscopy system (a); PL and Raman spectroscopy system model Jobin Yvon HR800UV (b) 64

Figure 3.19. A typical PL spectrum (a); a typical Raman spectrum (b) 65

Figure 3.20. Typical UV-Vis transmission spectrum; the bandgap energy of the sample is determined from the intersection of linear interpolation of spectrum and x-axis [107].. 66

Figure 3.21. Optical reflectometry system (Filmetrics F20)..................................... 67

Figure 3.22. Schematic optical diagram of a Fourier-transform infrared (FT-IR) spectrometer (a); FT-IR spectrometer model PerkinElmer (b) 67

Figure 3.23. Schematic diagram of an MSM structure connected to a SourceMeter instrument for *I–V* measurements (a); a schematic of metal Schottky contacts based on a porous structure (b) 68

Figure 4.1. Cyclic voltammogram plots for the electrochemical etching of n-type silicon in a hydrofluoric acid (HF) based solution under visible light and in the dark. The potential was scanned at a rate of 20 mV/s. 71

Figure 4.2. SEM images of porous samples *A*, *B* and *C* with delay times of 0, 2, and 4 min. Cross sectional micrographs are shown by A1, B1 and C1 respectively 73

Figure 4.3. PL spectra of porous samples *A*, *B*, *C* and non-porous Si (c-Si) 74

Figure 4.4. Raman spectra of samples *A* (no T_d), *B* (2 min T_d), *C* (4 min T_d) and c-Si 76

Figure 4.5. FT-IR spectra of the PS samples *A* (T_d = 0 min), *B* (T_d = 2 min), and *C* (T_d = 4 min). 78

Figure 4.6. Current–voltage characteristics of fabricated MSM photodetectors measured in the dark (I_{Dark}) and under illumination (I_{Ph}); Inset is the current gain (I_{Ph}/ I_{Dark}) 79

Figure 4.7. Cyclic performance of MSM photodetectors based on samples *A* (no T_d), *B* (2 min T_d), and C (4 min T_d) for a constant voltage of 5 *V* exposed to a pulsed visible illumination 81

Figure 4.8. The planar (a) and cross-sectional (b) SEM micrographs of thermally carbonized porous silicon 84

Figure 4.9. Energy Dispersive X-ray (EDX) spectra of PS and TC-PS samples 85

Figure 4.10. Fourier Transform Infrared (FT-IR) spectra of the PS sample prior and after carbonization 86

Figure 4.11. PL spectra of porous silicon prior carbonization (PS) and after that (TC-PS), under continuous exposure of low power laser radiation for 0, 20 and 40 min 88

Figure 4.12. The I–V characteristics of MSM photodetectors based on PS and TC-PS under continuous exposure of low power laser radiation at regular intervals of 30 min 89

Figure 4.13. The ratio of photocurrent to dark current (gain) under continuous radiation of laser at regular intervals for freshly prepared porous silicon (PS) and thermally carbonized porous silicon (TC-PS) samples. 90

Figure 5.1. Cyclic voltammogram plots for the electrochemical etching of n-type 6H-SiC in a hydrofluoric acid (HF) based solution under ultraviolet (UV) light and in the dark. The potential was scanned at a rate of 20 mV/s. 94

Figure 5.2. Planar SEM images of PSC samples prepared via UV-assisted electrochemical etching under different current densities: (a) 10, (b) 15, and (c) 20 mA/cm^2. Cross sectional micrographs are shown by (a1), (b1) and (c1) respectively. 97

Figure 5.3. Three-dimentional view of AFM images in the scale of 10*10 μm^2 from PSC samples prepared via UV-assisted electrochemical etching of n-type 6H-SiC under different current densities: (a) 10, (b) 15, and (c) 20 mA/cm^2 98

Figure 5.4. Optical transmission spectra of PSC *A* (J = 10 mA/cm^2), *B* (J = 15 mA/cm^2), and *C* (J = 20 mA/cm^2); the dotted line shows intersection with x-axis to determine optical bandgap. Inset is the average transmission percentages and measured band gaps for the different porous layers 99

Figure 5.5. PL spectra of the PSC samples etched at different current densities: 10 mA/cm^2 (PSC *A*), 15 mA/cm^2 (PSC *B*), 20 mA/cm^2 (PSC *C*), and non-porous SiC (6H-SiC). 101

Figure 5.6. Raman spectra of (a) non-porous 6H-SiC, and porous SiC etched under different current densities: (b) 10, (c) 15, and (d) 20 mA/cm^2 in the 200 cm^{-1} to 600 cm^{-1} range (A) and in the 600 cm^{-1} to 1100 cm^{-1} range (B). 103

Figure 5.7. *I*-*V* characteristics of fabricated UV photodetectors on PSC substrates with different current densities: 10 mA/cm^2 (PSC *A*), 15 mA/cm^2 (PSC *B*), 20 mA/cm^2 (PSC *C*) in dark (I_d) and under UV illumination (I_{ph}). Inset shows the current gain (I_{Ph}/I_d). 106

Figure 5.8. Responsivity spectra of the PSC photodetectors. Inset is the calculated quantum efficiency. 107

Figure 5.9. Cyclic performance of MSM UV photodetectors based on PSC *A* (J = 10 mA/cm^2), *B* (J = 15 mA/cm^2), and C (J = 20 mA/cm^2) for a constant voltage of 5 *V* exposed to a pulsed UV illumination 108

Figure 6.1. A three-dimensional SEM micrograph of porous-shaped SiC based on TC-PS template (a); a schematic diagram of MSM photodetector based on porous-shaped SiC/TC-PS sample (b) 112

Figure 6.2. Planar view of the scanning electron microscope (SEM) images of (a) thermally carbonized porous silicon (TC-PS) and sputtered porous-shaped silicon carbide on the TC-PS substrate at different annealing temperatures: (b) 800 , (c) 1000 , and (d) 1200 °C. 114

Figure 6.3. Cross-sectional view of field-emission SEM (FESEM) images of (a) TC-PS and sputtered SiC samples on the TC-PS substrate at different annealing temperatures: (b) 800, (c) 1000 and (d) 1200 °C. 115

Figure 6.4. Energy-dispersive X-ray spectrometry (EDX) of PS, TC-PS, and SiC/TC-PS samples 116

Figure 6.5. X-ray diffraction (XRD) spectra of the sputtered SiC on the TC-PS substrate (a) before annealing and after annealing at (b) 800, (c) 1000, and (d) 1200 °C 118

Figure 6.6. Reflection spectra of the TC-PS substrate and sputtered porous-shaped SiC on the TC-PS substrate before and after annealing at different temperatures 120

Figure 6.7. Photoluminescence (PL) spectra of (a) the TC-PS substrate, (b) sputtered samples before annealing and after annealing at (c) 800, (d) 1000, and (e) 1200 °C in the 350 nm to 570 nm range. The inset shows the PL spectrum of the TC-PS substrate in the 350 nm to 950 nm range. 121

Figure 6.8. Raman spectra of (a) the TC-PS substrate and the sputtered SiC (b) before annealing and after annealing at (c) 800, (d) 1000, and (e) 1200 °C within the 400 cm^{-1} to 1100 cm^{-1} range. 124

Figure 6.9. Current-voltage characteristics of fabricated UV detectors on sputtered SiC substrates with different annealing temperatures; Inset is the current gain (I_{Ph}/ I_d) 126

Figure 6.10. Responsivity spectra of Ni/SiC/TC-PS UV detectors with different annealing temperatures; inset is the calculated values of quantum efficiency. 128

Figure 6.11. Cyclic performance of ultraviolet photodetectors based on SiC samples with different annealing temperatures for a constant voltage of 5 *V* exposed to a pulsed UV radiation. 129

LIST OF SYMBOLS

a	Lattice constant
A	Area
A^{**}	Richardson's constant
c	Lattice constant
d	Interplanar spacing of the crystal planes
D	Average crystal size
e	Charge of electron
E_C	Conduction band
E_F	Fermi level of semiconductor
E_g	Semiconductor band gap
E_v	Valence band edge
(hkl)	Miller indices
G	Current gain (contrast ratio of photo and dark currents)
I	Current
I_o	Saturation current
J	Current density
k	Boltzmann constant
m_o	Electron mass
m^*	Effective mass
n	ideality factor
P	Porosity
q	Electron charge

R	Responsivity
S	Sensitivity
t	Time
T	Absolute temperature
V	Voltage
w	Width
α	Absorption coefficient
ε_a	Strain along a-axis
ε_c	Strain along c-axis
σ	Conductivity
ν	Frequency
θ	Incident / Diffraction angle
χ	Semiconductor electron affinity
φ_B	Schottky barrier height
ϕ_M	Metal work function
ϕ_S	Semiconductor work function
μ_n	Electron mobility
μ_p	Hole mobility
ρ	Resistivity
λ	Wavelength
η	Quantum efficiency
T_{on}	Working time
T_{off}	Pause time
T_{d}	Delay time

LIST OF MAJOR ABBREVIATIONS

a.u.	Arbitrary unit
AFM	Atomic force microscopy
CE	Counter electrode
CV	Cyclic voltammetry
CVD	Chemical vapor deposition
DC	Direct current
EDX	Energy dispersive X-ray
eV	Electron volt
FESEM	Field-emission scanning electron microscopy
FT-IR	Fourier-transform infrared spectroscopy
FWHM	Full width at half maximum
IC	Integrated circuit
ICDD	International centre for diffraction data
I-V	Current-Voltage
LA	Longitudinal acoustic
LED	Light emitting diode
LO	Longitudinal optic
LPE	Liquid phase epitaxy
M	Metal
MBE	Molecular beam epitaxy
MOCVD	Metalorganic chemical vapor deposition
MS	Metal-semiconductor

MSM	Metal-semiconductor-metal
PD	Photodetector
PDF	Powder diffraction file
PS	Porous silicon
PSC	Porous silicon carbide
PEC	Photoelectrochemical
PVD	Physical vapor deposition
PL	Photoluminescence
RE	Reference electrode
RCA	Radio Corporation of America
RMS	Root mean square
RF	Radio frequency
SBH	Schottky barrier height
sccm	Standard cubic centimetres per minute
SEM	Scanning electron microscopy
TA	Transversal acoustic
TC	Thermal carbonization
TC-PS	Thermally carbonized porous silicon
TO	Transverse optic
UHV	Ultra high vacuum
UV	Ultraviolet
UV-Vis	UV-Visible spectroscopy
WE	Working electrode
XRD	X-ray diffraction

PERKEMBANGAN NANOSTRUKTUR SILIKON DAN SILIKON KARBIDA UNTUK APLIKASI FOTONIK

ABSTRAK

Dalam kajian ini, ciri-ciri struktur, optik, dan elektrik nanostruktur silikon dan silikon karbida telah dibangunkan untuk aplikasi fotonik. Foto-pengesan yang tampak jelas dan bersifat ultra-ungu (UV) difabrikasi berdasarkan kepada nano-struktur silikon poros (PS) dan silikon karbida poros (PSC) yang dioptimakan. Dalam kategori pertama kajian ini, sampel-sampel PS yang mempunyai keporosan dan keseragaman yang tinggi dikeluarkan menggunakan satu kombinasi inovatif teknik-teknik punaran foto-elektrokimia tanpa-elektrik dan berdenyut. Punaran kimia tanpa elektrik dioptimakan dengan mengaplikasikan waktu penangguhan selama 2 minit sebelum proses elektrokimia untuk mendapatkan keporosan (83%) dan keseragaman yang paling tinggi dan seterusnya meningkatkan ciri-ciri foto-luminar (PL). Seterusnya, karbonisasi haba sampel-sampel PS yang baru sahaja disediakan dijalankan untuk menstabilkan ciri-ciri optik dan elektrikal. Dalam kategori kedua, sampel-sampel PSC yang mempunyai keporosan dan keseragaman yang tinggi disintesiskan melalui pengoptimaan kepadatan semasa punaran. Sampel yang dioptimakan (J = 20 mA/cm^2) menunjukkan keporosan permukaan yang tertinggi (76%), kekasaran permukaan tertinggi (137 nm), puncak PL yang mempunyai keamatan tertinggi, dan kestabilan tertinggi berbanding dengan sampel-sampel PSC yang lain. Dalam kategori ketiga, lapisan nipis yang mempunyai keporosan yang tinggi dan berbentuk poros sekata dibiakkan berdasarkan kepada substrat TC-PS menggunakan pemercikan magnetron RF. Proses pasca-penyepuhlindapan pada suhu 1200 °C menambahbaiki keseragaman, saiz bijirin (1380 nm), kekasaran permukaan (610 nm), dan keamatan PL (237.3 a.u.). Pengesan-pengesan foto seterusnya difabrikasi dengan membuang hubungan Schottky ke atas semua sampel poros. Keputusan-keputusan menunjukkan bahawa nano-struktur silikon dan silikon karbida yang sudah dioptimakan, dengan keporosan dan keseragaman yang tinggi adalah bahan-bahan yang sesuai untuk pengesanan foto yang bersifat boleh-nampak dan ultra-ungu.

DEVELOPMENT OF SILICON AND SILICON CARBIDE NANOSTRUCTURES FOR PHOTONIC APPLICATIONS

ABSTRACT

In this study, the structural, optical, and electrical properties of silicon and silicon carbide nanostructures are developed for photonic applications. Visible and ultraviolet (UV) photodetectors are fabricated based on optimized porous silicon (PS) and porous silicon carbide (PSC) nanostructures. In the first category of this work, the high-porosity and uniform PS samples are generated using an innovative combination of electroless and pulsed photoelectrochemical etching techniques. The electroless chemical etching is optimized by applying the delay time of 2 min prior to the electrochemical process to obtain the highest porosity (83%) and uniformity and hence enhanced photoluminescence (PL) intensity. Next, thermal carbonization of freshly-prepared PS samples is carried out to stabilize their optical and electrical characteristics. In the second category, the high-porosity and uniform PSC samples are synthesized through optimization of etching current density. The optimized sample (with J = 20 mA/cm^2) shows the highest porosity (76%), highest surface roughness (137 nm), the most intense PL peak, and the highest stability compare to the other PSC samples. In the third category, high-porosity and uniform porous-shaped SiC thin films are grown based on TC-PS substrates using RF magnetron sputtering. The post annealing process at 1200 °C improves uniformity, grain size (1380 nm), surface roughness (610 nm), PL intensity (237.3 a.u.) and Raman red-shift (24 cm^{-1}). Photodetectors are subsequently fabricated by depositing Schottky contacts onto all porous samples. The results show that the optimized nanostructures of silicon and silicon carbide with high porosity and uniformity are suitable materials for visible and UV photodetection.

CHAPTER 1

INTRODUCTION

1.1 Fundamentals of Compound Semiconductors and Silicon Carbide

Compound semiconductors have been a subject of electronic research for nearly as long as elemental semiconductors. Germanium was initially discovered in the late 1940s and early 1950s [1]. Over time, germanium has been replaced by silicon, which is a more robust, reliable, and technologically well-behaved material with stable oxides [2]. Compound semiconductors, whose merit of superior transport was recognized as early as in 1954 by Welker [3], have continued to be of interest since these early days. The areas of significant applications include light sources, microwave sources, microwave detectors, visible, and visible-blind photodetectors [4]. All of these applications are areas of semiconductor research to which compound semiconductors are uniquely suited. The specific characteristics of some compound semiconductors, such as wide bandgap, elevated melting point, and chemical stability, make them more favorable for operation in harsh environments than elemental semiconductors.

Silicon carbide (SiC) is a wide bandgap semiconductor with many superior mechanical and electrical properties compared with Si [5]. These properties include high electron mobility (1000 $cm^2/V\cdot s$), elevated electron saturation velocity (2.0×10^{17} cm/s to 2.7×10^{17} cm/s), elevated breakdown electric field (2×10^6 V/m to 3×10^6 V/m), high decomposition temperature (2830 °C), high thermal conductivity (3.6 W/cm·K to 4.9 W/cm·K), and very low thermal expansion coefficient (4.0×10^{-6}/K) [6]. The range of possible wide bandgaps in SiC polytypes are also desirable for switches in electric power distribution systems, high-

temperature turbine engines, high-frequency power devices, high-temperature ambient detectors, and detectors for various harsh environments [7]. The elevated sublimation temperature of SiC makes it an applicable material for furnace parts. SiC does not melt at any pressure and is highly inert chemically. Moreover, SiC is the substrate of choice in the production of light-emitting diodes in the ultraviolet (UV) and blue range of the spectrum [8] because of its low lattice mismatch and low thermal expansion coefficient for GaN epitaxial layers. SiC-based UV detectors can also be used in various applications, such as in monitoring combustion processes, water purification systems, and detection of photochemical phenomena given that detectors are almost solar-blind [9]. The transparency of SiC at wavelengths higher than its band gap makes it a useful material for the fabrication of photodetectors capable of rejecting visible and near infrared regions of the spectrum while providing near-unity efficiency in the UV range [10]. Many properties of semiconductors are determined by their crystalline structure. Figure 1.1 illustrates the major polytypes of SiC.

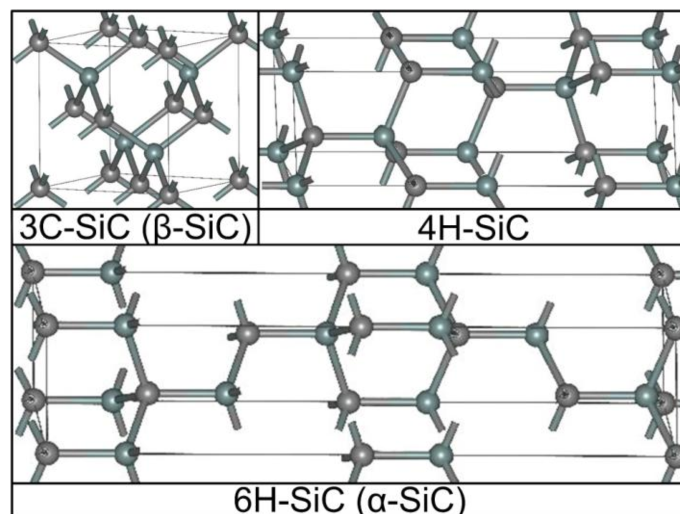

Figure 1.1. Structure of SiC polytypes

Alpha SiC (α-SiC) is the most common polytype; it has a hexagonal structure (same as Wurtzite). The beta modification (β-SiC), has a zinc blende (cubic) structure (same as diamond). The beta structure has had relatively less commercial uses. However, its higher surface area than the hexagonal structure has increased its applications as a support for heterogeneous catalysts [11]. Figure 1.2 shows the structure of major hexagonal SiC polytypes.

Here, three SiC bilayer structures (that is, three atoms with two bonds) are shown and labeled as A, B, and C. Using these A, B, and C elements, any SiC polytype can be defined as shown in Figure 1.2 on example of the hexagonal structures 2H, 4H, and 6H. The 2H-SiC structure includes only elements A and B stacked as ABABAB. The 4H-SiC structure is twice longer and the second half is twisted compared with 2H-SiC, producing the ABCB structure. The 6H-SiC unit cell is three times longer than 2H, and the structure is ABCACB. The letters H and C denote the hexagonal and cubic symmetries, respectively. Table 1.1 shows the physical properties of the different SiC polytypes.

Table 1.1. Physical properties of major SiC polytypes [12].

Polytype	Crystal structure	Lattice constant (Å)	Density (g/cm^3)	Bandgap (eV)
3C (β)	Zinc blende (cubic)	4.3596	3.21	2.36
4H	Hexagonal	3.0730; 10.053	3.21	3.23
6H (α)	Hexagonal	3.0730; 15.11	3.21	3.05

The production technology for high quality SiC material only became successful after 1990. At present, wafers of up to 150 mm diameter are commercially available with highly uniform epitaxial layers as thick as 100 μm [13]. The currently

available high quality SiC material makes possible a variety of SiC for a broad range of research and device fabrication.

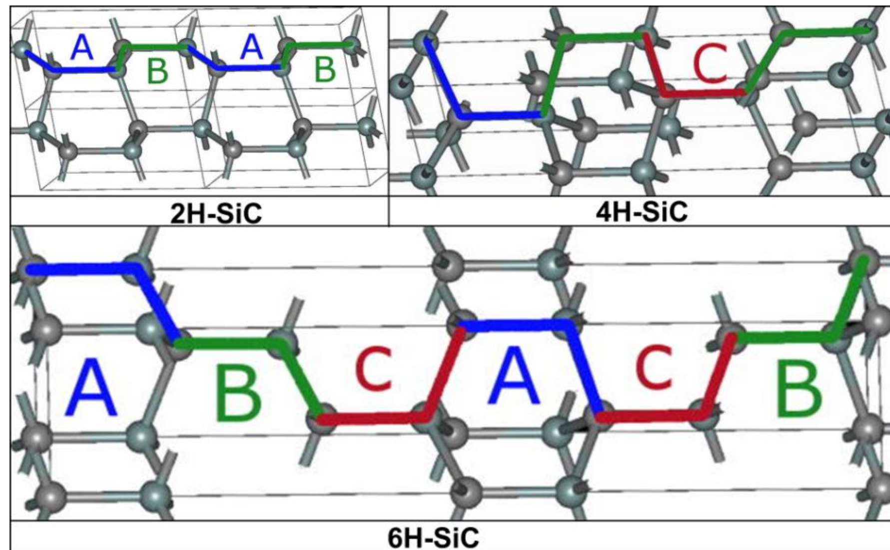

Figure 1.2. Structure of major hexagonal SiC polytypes

1.2 Overview and Background of Porous Silicon and Porous SiC Nanostructures

Nanostructures are those materials with at least one dimension with the nanometer scale. These include nanoparticles (0D), nanowires (1D), and thin films (2D). Recently, nanostructured materials have received considerable attention due to their special physical properties that are widely different from those of their bulk phases. Their properties are strongly dependent on the structure type, dimension, and surface nature [14]. Controlling the properties of these materials by varying these parameters can be done for technological applications such as optoelectronics and sensing. Porous nanostructures are one of the known nanostructured materials. The description of porous implies that billions of micro and nano-sized holes are formed

inside the materials. The ratio of voids' volume to the total volume is called the porosity [15].

Porous semiconductors are one of the most common porous materials, which have promising optoelectronic applications. The tunable physical properties, large surface-to-volume area, and band gap broadening are some of their properties that can be used for sensing applications [16]. Recently, the request for more sophisticated and powerful devices has led to studies on the fabrication of compound semiconductors on porous substrates. The most outstanding advantage of porous semiconductors for substrate applications is that the nanopatterned porous structures can act as a sink to accommodate the strain and threading dislocations to obtain the subsequent layer with lesser dislocation densities and strain [17].

Porous silicon (PS) has been considered an advantageous material for sensing applications since the discovery of its efficient visible room temperature photoluminescence (PL). A successful experiment was published in the 1990s revealed that electrochemical and chemical dissolution enabled the silicon wafers to emit light in red luminescence [18]. Moreover, Canham et al. [19] argued that PS may display the quantum confinement effects of carriers on the silicon nanocrystals present in the pore walls. The publication of these results elicited increasing interest in PS, particularly in its non-linear optical properties. A number of studies were devoted to the properties and potential applications of PS, and investigations on this element continued to increase, especially between 1991 and 1995 [20]. The compatibility of PS with Si-based electronic circuits has been considered a motivation for the development of PS-based technologies [21]. PS substrates have large surface areas of 200–500 $m^2 cm^{-3}$ and therefore, they have high reaction

activities in their surfaces. Many investigations have indicated that the optical and electrical characteristics of PS may considerably change by adsorption of different molecules onto their surfaces [22, 23]. Consequently, PS substrates are high-potential sensing materials capable of increased adsorptive effects [24]. The sensitivity of PS-based devices depends on the morphological properties of its pores, i.e., surface regularity, diameter and uniformity, as well as layer thickness [25].

Although PS has attracted considerable attention, its chemical, thermal, and mechanical instabilities hinders its high rate of application [26]. These problems have led to the further studies on other porous semiconductors, such as GaP, GaAs, and InP, as well as the wide band gap semiconductors, like GaN and SiC. Porous SiC (PSC) has become the focus of considerable attention because of its large internal surface area and high activity in surface reactions. Consequently, PSC layers are used as high-potential sensing materials because of their enhanced adsorptive properties [27]. In addition, the remarkable PL intensity and stability of the physical and chemical properties of PSC may expand their applications compared with the PS substrates [28, 29].

Etching is an essential technique for the formation of porous semiconductor samples. To date, dry etching methods such as inductively coupled plasma and electron cyclotron have been mostly applied [30, 31]. However, these methods require expensive and sophisticated techniques and have a high risk of damaging the surface [32-35]. Thus, wet-chemical etching is a useful alternative in many cases [36]. Wet chemical etching of semiconductor substrates involves two main methods, namely, metal-assisted electroless chemical etching and electrochemical etching. The former suffers from the lack of controllability of the pore size and distribution,

whereas the latter technique, which was pioneered by Shor et al. [37, 38], can be controlled through several parameters, such as current density, voltage, electrolyte composition, and illumination conditions. Konstantinov et al. [39] investigated the physical characteristics and the formation process of porous SiC produced by photoelectrochemical etching as well as the dark etching and proposed the model of self-regulation of the fiber size. In 2000, Zangooie et al. [40] followed up with studies on different pore morphologies and possible formation mechanisms of SiC.

However, many of the reproducible morphologies of porous templates, which were discovered in 2004, did not serve the needs of high-efficiency photonic applications. In the current research, a novel pulsed-current photo-electrochemical etching process that can control the porosity of PS and PSC substrates is introduced. This process is controlled by electrical etching parameters such as delay time and current density. The main topic of this research is the fabricated high-quality and uniform porous structures, which have made breakthroughs in photonic applications.

1.3 Overview and Background of SiC Growth Techniques

Although the use of SiC is relatively new in the electronics industry, it has long been used as a material for other purposes. SiC formation was first reported in 1824, recognized as a silicide of carbon (C). In 1893, SiC was successfully synthesized by the Acheson process [41] using sand and coke. However, reports on the development of SiC as a semiconductor material until 1955 were unavailable because of the difficulties of forming high quality single crystals. In 1955, Lely showed the growth of SiC on a PSC using vapor condensation method. This technique was further developed by Hamilton et al. [42] and Novikov et al. [43] and is referred to as the Lely technique. Kendal [44] proposed a technique of cracking

gaseous compounds containing Si and C to form SiC crystallites at high temperatures. This method is probably the fundamental for today's chemical vapor deposition (CVD) method. An important breakthrough occurred in 1978 when Tsvetkov and Tairov [45] demonstrated the seeded growth of SiC by sublimation technique. Their study was the milestone for SiC growth technology. Given that Tairov and Tsvetkov used Lely's theory of vapor condensation, their technique is known as the modified Lely method. SiC wafers were first produced commercially by Cree Research, Inc., in 1991. The availability of SiC wafers in recent years is due to the extensive research on SiC epitaxial growth. To enhance the quality of bulk material and to fabricate sophisticated device structures, epitaxial methods are applicable. Considerable efforts have been made recently for epitaxial growth of SiC thin films by various conventional growth techniques. The epitaxial techniques can be categorized based on the phase (vapor or liquid) of the material used to form the epitaxial layer. Growth techniques include liquid phase epitaxy (LPE), chemical vapor deposition (CVD), molecular beam epitaxy (MBE), and physical vapor deposition (PVD). In this section, we briefly present these techniques.

1.3.1 Liquid Phase Epitaxy (LPE)

LPE is a method for the formation of the epitaxial thin films from saturated solutions. The chosen solvent has generally low vapor pressure and low melting point. LPE method is mostly applied for the growth of compound semiconductors. High quality, thin and uniform layers can be grown by this technique. SiC does not make a stoichiometric liquid formation at normal physical conditions. Instead, the material decomposes to vapor at 2830 °C. Therefore, the growth of SiC can be performed using a non-stoichiometric melt [46]. Si is the preferred choice for the

solution because it is a constituent of SiC. Moreover, high-quality Si is commercially available. The growth rate using Si as a solvent is not high because the solubility of carbon in silicon is low at temperatures less than 2000 °C. By adding a transition metal to the silicon melt, the solubility of carbon is enhanced. For instance, silicon–scandium (Si–Sc) melts has demonstrated perfect influence on the growth rate of SiC as well as on the structural characteristics (surface morphology and crystallinity) of the SiC epitaxial layers [5]. Generation of micropipes is a critical issue in SiC bulk crystal growth. The existing micropipes in the surface of the material can be closed using LPE growth technique [47]. The main advantage of LPE technique is that the growth temperature can be well below the melting point of the deposited material. Moreover, the equipment is inexpensive, simple, and non-hazardous. The key problem of LPE technique for the formation of the epilayer is that this method is too simple to deposit sophisticated nanostructured materials due to the difficult composition and thickness control.

1.3.2 Chemical Vapor Deposition (CVD)

Generally, CVD is a process in which high quality thin layers of intrinsic or doped layers of semiconductors can be grown. The substrate is heated to high temperatures where chemical decomposition, called pyrolysis of a gas, generally takes place directly on the surface of the heated substrate. Homo-epitaxial CVD deposition of SiC has been reported on 3C, 4H, and 6H polytypes of SiC, whereas hetero-epitaxy of 3C-SiC has been reported on sapphire, Si, AlN, and 6H-SiC substrates [48]. Scientists from North Carolina State University introduced a growth technique employing the SiH_4–C_2H_4–H_2 gas system. In the epitaxial growth method described at NASA Lewis Research Center for 4H-SiC and 6H-SiC, the substrates

are first etched by HCl at 1350 °C prior to growth. The initial HCl cleaning procedure decreases the density of surface defects in the deposited SiC epitaxial layers.

The surfaces of SiC CVD layers may contain large amounts of imperfections. Surface defects observed in SiC epitaxial layers are polytype inclusions (which appear as triangular features), growth pits, micropipes, and macro-steps (often referred to as step bunching) [49]. The sizes of some defects are relatively large (tens of microns), whereas others have an average size less than 1 µm. Although many researches have been performed in understanding the nature of structural defects, the control and origin of many defects in SiC remain to be investigated.

1.3.3 Molecular Beam Epitaxy (MBE)

In 1958, MBE was described by Gunther [50] as a technique of growing compounds on heated substrate by evaporation from two sources. In 1975, Cho and Arthur [51] achieved major developments toward modern MBE equipment. The growth chamber is the heart of an MBE system. During the fabrication process, elemental materials are heated in Knudsen cells and evaporated onto a substrate under ultra-high vacuum (UHV) conditions ~10^{-10}–10^{-11} Torr. The UHV growth ambient is crucial to the MBE process. It provides a clean growth environment leading to deposited layers with a high purity, which is very important for the deposition of high-quality semiconductors used for high-performance electronic devices. MBE growth has a number of benefits such as hetero-polytype growth (for instance 4H/3C/4H heterostructure), deposition of atomically abrupt interfaces, and in situ characterization. However, this method is rarely used for SiC growth because of its high costs and source material availability. Si source is widely available, but C

is not easy to obtain. Graphite can be applied, but high temperatures are required. C_{60} does not require high temperature cells, but the material is costly. For gaseous precursor usage, many technical problems arise, such as keeping UHV and high temperature requirement (>1200 °C), which makes this technique hard to use.

1.3.4 Physical Vapor Deposition (PVD)

Physical deposition techniques, such as radio frequency (RF) magnetron sputtering, use ion irradiation to induce film growth [52]. The sputtering process usually works at moderate vacuum around 2×10^{-2} mbar where the pressure of the sputtering gas remains stable. Argon is used as a sputtering gas because it is inert. In this process, the gas atoms are ionized and bombard the target. The different potentials between the target and the substrate holder make the gas ions move toward the target and make collision. Accordingly, the sputtered atoms can ballistically move from the source in straight path and impact energetically on the substrates. Alternatively, at high gas pressures, the sputtered atoms collide with the gas atoms and fly diffusively; reaching the substrates and condensing after undergoing a random fly. The whole range from energetic ballistic impact to low-energy thermalized motion is reachable by changing the background gas pressure [53]. RF sputtering can be used for epitaxial growth of metals and insulators. This technique can be very easily controlled because it is independent from many of the experimental parameters. The quality of sputtered layers can also be optimized by controlling many parameters including substrate temperature, working pressure, RF power, time of deposition, and so on. RF magnetron sputtering is a novel deposition technique to grow thick SiC thin films with an elevated growth rate. The process is based on sublimation of a SiC source and transport of vapor species to the substrate

surface. In sputtering technique, a solid SiC target is used instead of a conventional SiC powder. Therefore, disturbances due to the irregular shape of the powder are avoided. In SiC epitaxy, pre-treatment of the target surface prior to growth is commonly needed. However, in sputtering, this is inherent by a surface removal through initial sublimation of the target surface at temperature increasing to temperature growth. These characteristics enable epitaxial growth of 4H-SiC and 6H-SiC layers with uniform surfaces, even in thick material. The technology is safe because no hazardous gases are used. Moreover, no clean area is needed, the loading procedure is simple, and no costly parts with protective coating (as needed in CVD) are required. The growth containers do not degrade even after many times of growth, and the basic technology is not complicated. These characteristics make the system less costly, and the growth costs mostly depend on the target costs.

In conventional epitaxial methods, hydrogen molecules penetrate into the deposited layers, resulting in the fabrication of a SiC:H thin film. The hydrogen is evaporated during thermal annealing, leading to the formation of numerous voids of hydrogen molecules. Therefore, thermal processing leads to the degradation of the thermal stability of SiC thin films that are fabricated using these methods [54]. RF magnetron sputtering has the advantage of producing SiC without a hydrogen precursor [55]. Therefore, it can provide high quality and high purity SiC thin films.

1.4 Overview of Semiconductor Photodetectors

Photodetectors are fundamentally semiconductor devices that convert optical energy (light) into electrical energy, which is mostly manifested as photocurrent. High-sensitivity and high-speed photodetectors have been widely studied over the past 10 years because of their application in optical generation of high power

microwaves and optical communication networks. First studies on photodetectors can be dated back to 1873 when Smith discovered photoconductivity in selenium [56]. The progress of photodetectors was slow until Einstein explained the observed photoelectric effect in metals, and Planck solved the black body emission problems by introducing the hypothesis of quanta. The performance of the photodetector depends on the distribution and flux of incident light as well as on electronic parameters of substrate material, such as doping levels and band structures [57]. Based on the application, the performance of photodetectors refers to sensitivity, wavelength selectivity, response and recovery times, and quantum efficiency [58].

Different kinds of photodetectors have been produced, such as Schottky diodes, p-n junctions, and metal–semiconductor–metal (MSM) structures [59-61]. MSM photodetectors have been popular in the field of optical communications in the past few years due to their several advantages. One of the most outstanding advantageous characteristics is its high response speed, which is a function of the geometry of the structure. The fundamental purpose of further developments in the field of MSM photodetector production is the improvement of physical characteristics.

Porous semiconductors can be assumed outstanding materials for light detection because of their vast surface area to volume ratio and high absorption coefficients. Different porous semiconductors with different band gap values provide a variety of photodetectors with different ranges of sensitivity. For example, PS is sensitive to visible light whereas PSC is sensitive to UV radiation and is visible blind [62].

1.5 Problem Statement

Several essential problems are addressed in this research, and they are summarized as follows: In recent years, many studies have been performed to fabricate uniform PS substrates for optoelectronic applications. However, the electrochemical etching has not been optimized completely and the porous structures suffer from lack of uniformity and controllability. These shortcomings are more critical when a high porosity of porous material is needed. In this study, a novel method of etching is introduced for fabrication of highly uniform PS substrates. This technique is based on a combination of chemical and electrochemical etching. The process can be adjusted by optimizing the duration of each process using a novel parameter, which is delay time. In this work, the delay time is optimized, and thus uniform thick PS samples are grown by applying a suitable ratio of chemical and electrochemical etching time. The instability of Si nanostructures is another concern for photonic applications of PS. Therefore, fabricated devices based on PS suffer from the lack of stability in case of commercializing this technology. This problem is minimized in this research by growing a protective layer on PS substrate. Our results show that thermal carbonization can stabilize the optical and structural properties of PS substrates and enhance the stability of fabricated photonic devices.

Although SiC has outstanding properties to withstand harsh environment, the excellent chemical stability and high hardness of this substrate make it difficult to etch in normal conditions. Some authors recommend molten potassium hydroxide (KOH) for SiC etching, which needs advanced experimental equipment and suffers from the lack of controllability. In this research, the electrochemical etching of SiC is optimized in hydrofluoric acid (HF)-based cell at room temperature. The uniformity

and porosity of the PSC samples are enhanced by optimizing the etching current density. Given that SiC is a high-cost material and optimization of electrochemical etching is an expensive technique because of the large amount consumption of substrate material, an inventive technique is introduced for the formation of porous-shaped SiC thin film on low-cost PS substrates. Here, the porous skeleton of PS is chosen as a template for growth of porous-shaped SiC with the same morphology. The SiC atoms were sputtered on PS substrate and followed the morphological characteristics of the PS template. Moreover, PS substrate is more suitable for SiC deposition comparing to Si substrate because it provides a lesser lattice mismatch. The results showed that this inexpensive product has the ability to compete with high-cost conventional PSC substrates, especially in photonic applications.

1.6 Research Objectives

In order to develop silicon and silicon carbide nanostructures for photonic applications, the following experimental objectives are set;

1. To develop the high-porosity, uniform, and stable porous silicon (PS) nanostructures by optimization of delay time in the photoelectrochemical etching technique.
2. To develop the high-porosity, uniform, and stable porous silicon carbide (PSC) nanostructures by optimization of current density in the photoelectrochemical etching technique.
3. To develop the high-porosity and uniform porous-shaped silicon carbide (SiC) nanostructures on stable PS using RF magnetron sputtering technique and optimization of post-deposition annealing process.

1.7 Scope of Study

This study optimized a photo-assisted electrochemical etching of silicon and silicon carbide to produce more uniform and stable porous semiconductor substrates. A novel porous-shaped SiC/PS structure is introduced for optoelectronic applications. The nanostructured materials were used to fabricate visible and UV photodetectors with enhanced performance.

1.8 Outline of Thesis

The content of this thesis is organized as follows: Chapter 1 deals with a literature overview of the research on silicon and silicon carbide etching and deposition and the main properties of these materials. The general principles and theories of the electrochemical etching, metal–semiconductor contact, porous formation mechanisms, RF-magnetron sputtering of SiC as well as the basic principles of photodetectors are covered in Chapter 2. Chapter 3 describes the methodology and instrumentation involved in this study.

The results obtained from the research works are analyzed and discussed in Chapters 4, 5, and 6. Chapter 4 discusses the results related to the photonic applications of the PS using a combinational etching method. Chapter 5 discusses the experimental results of the UV-assisted pulsed electrochemical etching of SiC and their optoelectronic applications. Chapter 6 discusses the results related to a novel technique for fabrication of porous-shaped SiC on PS substrate using RF-sputtering method. In this chapter, a high-photoconductive UV photodetector based on SiC/PS substrate is introduced. Chapter 7 presents the conclusions of our work and suggestions to future studies.

CHAPTER 2

LITERATURE REVIEW

2.1 Introduction

The principle that applies to photodetectors is the photoelectric effect, which is the effect on a circuit caused by light. In 1900, Max Planck discovered that energy is radiated in small discrete units called quanta. The photoelectric effect is the effect of light on a surface in a vacuum; the result is electrons being ejected from the surface. This phenomenon explains the principle theory of light energy that allows photodetectors to operate.

In this chapter, general principles and theories of all subjects involved in this work are presented. It starts with a brief explanation of photoelectrochemical (PEC) etching of semiconductors. The advantages and properties of PEC etching are reviewed, and the extension of this processing method to silicon and silicon carbide is addressed. The fundamentals of PVD of SiC and the mechanism of SiC growth are discussed. Moreover, the fundamentals of metal–semiconductor contacts and the basic principles of visible and UV photodetectors are briefly described in this chapter.

2.2 Principles of Photoelectrochemical Etching

The electrochemistry of semiconductor materials has played an outstanding role in the development of electronic devices such as integrated circuit (IC) technology. Many of the processes applied in IC fabrication are based on

electrochemical principles. Furthermore, electrochemistry is the foundation for understanding the basic mechanisms of deposition, etching, and corrosion.

The PEC etching of semiconductors is an area of particular interest. PEC is a research field that includes photo-assisted electrochemical reactions of semiconductors in contact with liquids, which are called electrolytes. When a semiconductor is immersed in an electrolyte, the electrons are exchanged between semiconductor surface and electrolyte because the Fermi level in the semiconductor is different from that of the electrolyte. In PEC etching, the potential of the semiconductor substrate is monitored using a power supply. At the same time, a source of light whose photon energy is higher than the bandgap energy of the semiconductor illuminates the semiconductor surface, resulting in formation of photogenerated electrons–holes pairs. The electrons and holes produced in the space-charge region near the surface are transported by two mechanisms: drift under the influence of the electric field and diffusion, which is caused by the carrier concentration gradient. These mechanisms facilitate the electrochemical etching of semiconductors.

2.2.1 Photoelectrochemical Etching Mechanism of Silicon

Since the first research of Canham [19], PS layers have mainly been obtained by PEC etching in aqueous or ethanoic HF. In this technique, pores are formed over a large area of Si surface using a complicated mix of electronic and chemical factors. Parameters like electrolyte composition, dopant type and concentration, applied current density, temperature, as well as light intensity with different wavelength all play roles, and many competing mechanisms are involved. However, the formation of PS can proceed through the following general steps: (1) pores uniformly nucleate

and with no particular order on the silicon surface; (2) current preferentially flows near the pore bottoms; (3) the pore walls become passivated, leading to the dissolution of silicon primarily at the PS/crystalline silicon substrate interface; (4) the pores do not redistribute or reconstruct; and (5) all samples contain a distribution of pore diameters rather than a single pore size. Figure 2.1 indicates a typical current density–voltage (J–V) curve for a diluted HF aqueous solution. The formation of pores occurs in the initial increasing part of the curve for $0 < V < V_{ep}$, where V_{ep} is the potential of the small sharp peak [63]. This peak, which is called the electropolishing peak, has a critical current that depends on the chemical composition in the solution and substrate. By increasing the potential for $V > V_{ep}$, the electropolishing of silicon occurs because of the formation of oxide layer on Si substrate. Therefore, if the current density remains less than J_{ep}, the pore formation is self-limited by the availability of holes within silicon walls. In this case, PS is formed [64].

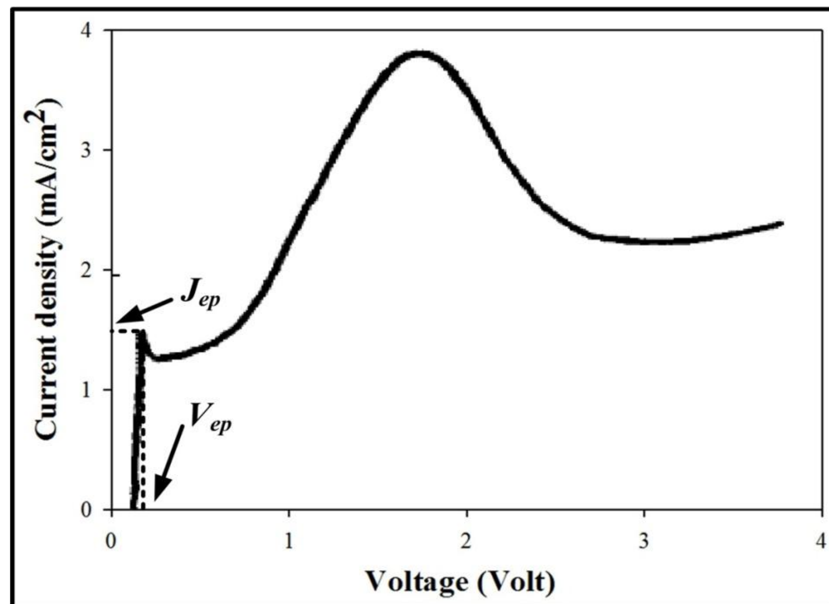

Figure 2.1. Typical J–V spectra of silicon in dilute aqueous HF solution. The porous layer is obtainable for $J < J_{ep}$. Adopted and redrawn from [65]

The chemical mechanism of electrochemical etching of silicon is shown in Figure 2.2. Generally, in the absence of an electron–hole pair, a hydrogen-saturated Si surface is free from attack of fluoride ions in the HF-based electrolyte. The Si-H structure is shown in Figure 2.2(A). In the next stage (B), a hole reaches the surface and attacks a Si-H bond. Therefore, a fluoride ion is replaced with a hydrogen atom, forming a Si-F bond. Next, the Si-F bond causes a polarization effect that allows a second fluorine ion to attack and replace the remaining hydrogen bond. Two hydrogen atoms can then combine and inject an electron into the substrate. Therefore, hydrogen gas is one of the products of the electrochemical etching of silicon. Figure 2.2(C) shows that in this reaction, two holes are required to remove one silicon atom from the crystal structure and to dissolve it in electrolyte. In stage (D), the polarization induced by the Si-F bonds reduces the electron density of the remaining Si-Si bonds, making them susceptible to attack by HF such that the remaining Si surface atoms are bonded with the hydrogen atoms. Finally, in stage (E), the Si tetrafluoride molecule reacts with HF to form the highly stable SiF_6 structure. The surface returns to its “neutral” state until another hole is made available [66]. The chemical reaction for etching of silicon can be summarized as follows [67]:

$$Si + 6HF \rightarrow H_2\mathrm{Si}F_6 + H_2 + 2H^+ + 2e^- \quad (2.1)$$

Therefore, a power supply is always needed to dissolve Si in this method. The final product is H_2SiF_6, which is relatively stable and can be easily dissolved in solution. In addition, the PEC etching current gradually decreases because of the increased density of hydrogen molecules near silicon walls, which does not allow fresh HF to react with the silicon surface. Therefore, electrochemical etching is a

self-controlled process. In the PEC process, photons absorbed from incident light create holes in Si. The criterion for photon absorption is that the photon energy of the incident light must be greater than or equal to the band gap of Si (1.12 eV). Therefore, light with a wavelength less than 1100 nm is suitable for creating minority charge carriers (holes) in silicon. Porous Si thin films are produced by irradiation with UV, visible, or infrared light on Si using HF solution. The wavelength of incident light and its power has a direct effect on the PEC etching of silicon.

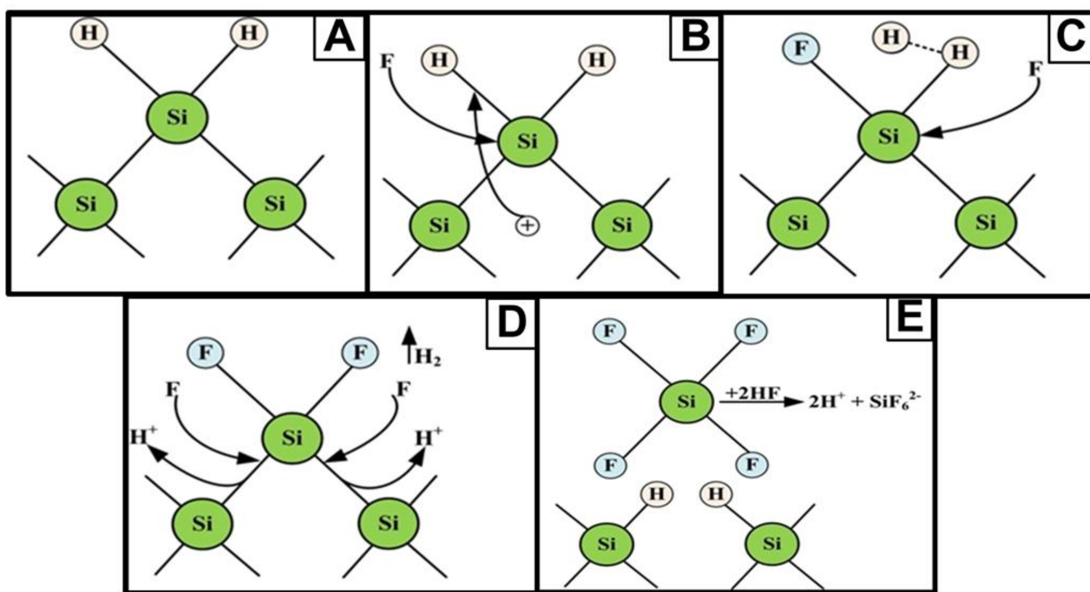

Figure 2.2. Schematic of the chemical dissolution mechanism of Si in HF solution. Adopted and redrawn from [66]

The photon absorption depth in Si is a function of the incident photon energy. Long-wavelength light is absorbed deeper in Si than short-wavelength light. When light with long wavelengths is used, the penetration depth in Si becomes higher or of the same magnitude as that of the thickness of the wafer. Thus, minority charge carriers (holes) can be created within the depletion region of Si and beyond the depletion region width.

2.2.2 Combinational Pulsed-Current Etching of Silicon

The photo-electrochemical etching method is an attractive technique for fabricating PS and producing optical waveguides. With this method, layers can be easily and uniformly fabricated over a large area of silicon substrate [68]. Pore morphology can also be controlled by optimizing several parameters, such as current density, etching time, light assistance, and ratio of chemicals in solution. PS is mostly formed by the constant current electrochemical anodization of Si in an HF-based electrolyte [69]. A typical etching process is very sensitive to the ratio of chemicals inside the cell. For example, acid is consumed during the chemical interactions in the pores, and its concentration near to PS walls thereby decreases, which negatively affects the etching process. Hydrogen bubbles generated in the pores also decrease the speed of etching, resulting in shallow pores [70]. The solution to this problem is the application of a discontinuous current combined with a cycle time (T) and a pause time (T_{off}). This method leads to the ejection of the H_2 bubbles and allows fresh HF molecules to react with Si substrate [71], where the HF concentration near the PS walls remains constant.

In the current research, a pulse-current technique by an innovative combination of electroless and electrochemical anodization of silicon substrate is studied. The electroless chemical etching is optimized by varying the delay time (T_d) prior to the electrochemical process to control the uniformity of the pores. The most acceptable reason for the evolution in the physical characterization of PS due to the application of delay time is the competition between the electroless chemical etching and anodic etching. The anodic etching of Si occurs when the holes reach the surface and initiate an electrochemical reaction. Chemical etching occurs when oxide forms

on the surface as a result of HOOH dissociation, which is followed by the chemical etching of the silicon oxide by HF. The latter process occurs throughout the reaction process, whereas the anodic etching only occurs when the current flows. When the oxide layer becomes uniform and covers the entire surface, electropolishing occurs. When only patches of oxide formed, the pores continue to grow. The additional T_d increased the relative portion of the chemical etching. During the delay, the crystalline silicon surface was affected by exposure to oxidant and etchant chemicals in the solution in the absence of a current. The electroless etching of silicon in fluoride solution occurred through the local coupling of redox reactions as follows [72]:

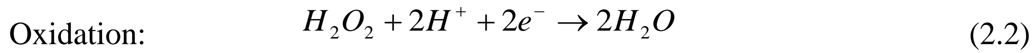

Oxidation: $$H_2O_2 + 2H^+ + 2e^- \rightarrow 2H_2O \quad (2.2)$$

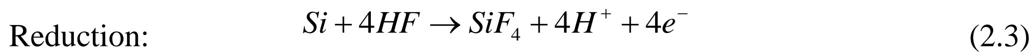

Reduction: $$Si + 4HF \rightarrow SiF_4 + 4H^+ + 4e^- \quad (2.3)$$

$$SiF_4 + 2HF \rightarrow H_2SiF_6 \quad (2.4)$$

Overall: $$Si + H_2O_2 + 6HF \rightarrow 2H_2O + H_2SiF_6 + H_2 \uparrow \quad (2.5)$$

The evolution of hydrogen bubbles during chemical etching proved the overall redox equation. During chemical etching, the entire silicon surface has equal etching parameters, e.g., concentration of acid and oxidant. This situation leads to homogeneous pore fabrication by the random localization of oxide islands. During electrochemical etching, electron flow is not uniform throughout the surface, resulting in non-uniform, sub-micrometer pore fabrication. Therefore, electroless etching can be assumed as a chemical method for fabricating shallow but uniform holes on silicon surfaces to be used as templates for fabricating deep and homogeneous pores. This depth and homogeneity are achieved by extending the

pores through the electrochemical etching process. However, increased T_d can lead to the growth of a uniform oxide layer, which causes the electropolishing of silicon surfaces, and results in shallow pores. Therefore, the optimum duration of T_d should be chosen to be applied prior to electrochemical etching in order to fabricate a uniform PS layer.

2.2.3 Principles of Photoelectrochemical Etching of SiC

None of the known etchants for silicon are found to chemically etch SiC at room temperature. Faust et al. [73] studied the reagents that attack SiC at temperatures near 1000 °C. He also summarized the electrolytic dissolution of SiC carried out at room temperature. Systematic researches on electrochemical etching of SiC were initiated decades later, in the 1990s [74]. Shor et al. [74] then showed that PSC can be formed by anodizing single crystalline 6H-SiC wafers in HF under UV light. UV is the only suitable radiation for producing the minority of carriers for the electrochemical etching of SiC, which has a high band gap of ~ 3 eV [75]. The role of UV radiation in enhancing the etch rate is partial because of the relatively shallow absorption depth of UV light [76]. This phenomenon allows more carriers to be photogenerated in the space charge layer. The UV light with the photon energy higher than the band gap energy of semiconductor produces electron–hole pairs. The electrons are swept away by the electric field into the bulk of the semiconductor, whereas the holes move to the surface where they take part in the electrochemical reaction. The UV-assisted PEC etching of SiC is an attractive technique for the fabrication of PSC and the production of optical waveguides because of the ease with which layers can be fabricated over a large area of the substrate, as well as the uniformity of the porous layers [36]. The anodic etching of SiC can proceed through